Journal of Zhejiang University-SCIENCE A (Applied Physics & Engineering) 2022 23(7):564-578
www.jzus.zju.edu.cn; www.springer.com/journal/11582
E-mail: jzus_a@zju.edu.cn

Research Article

https://doi.org/10.1631/jzus.A2100683

Numerical analysis of the influence of a river on tunnelling-induced ground deformation in soft soil

Jia-xin LIANG[1,2], Xiao-wu TANG[1,2]✉, Tian-qi WANG[1,2], Yu-hang YE[1,2], Ying-jing LIU[3]

[1]*Research Center of Coastal and Urban Geotechnical Engineering, Department of Civil Engineering, Zhejiang University, Hangzhou 310058, China*
[2]*Engineering Research Center of Urban Underground Space Development of Zhejiang Province, Hangzhou 310058, China*
[3]*Zhongtian Construction Group Co., Ltd., Hangzhou 310020, China*

Abstract: When tunnels are constructed in coastal cities, they will inevitably undercross a river. Exploring the influence of rivers on tunnelling-induced deformation in costal soft soil is of great significance for controlling excessive settlement and protecting surrounding buildings. This paper presents a case study of twin tunnels undercrossing a river in soft soil in Hangzhou, China. The soft soil of Hangzhou refers to cohesive soil in a soft plastic or fluid plastic state with high natural water content, high compressibility, low bearing capacity, and low shear strength. Considering the influence of the river, the research region was divided into two parts, inside and outside the river-affected area, based on monitoring data of the Zizhi Tunnel. The development law of surface settlement is divided into three stages. In the first and second stages, the surface settlement within and outside the river-affected area showed a similar trend: the settlement increased and the growth rate of settlement in the second stage was smaller within the river-affected area. In the third stage, the surface settlement continued to increase within the river-affected area, while it converged outside the river-affected area. Within the river-affected area, there was an asynchronization of the sinking rate and stability of vault settlements and surface settlements. A numerical model was established by simulating different reinforcements of the tunnel. The numerical model revealed that the ground movement is influenced by the distribution and amount of the excess pore water pressure. The excess pore pressure was concentrated mostly in the range of $1.0H_t$–$3.0H_t$ (H_t is the tunnel height) before the tunnel face, especially within the river-affected area. Inside the river-affected area, the dissipation of excess pore water pressure needs more time, leading to slow stabilization of surface settlement. When undercrossing a river, a cofferdam is necessary to reduce excessive ground deformation by dispersing the distribution of excess pore water pressure.

Key words: Tunnelling; Ground deformation; Numerical analysis; Reinforcement

1 Introduction

More and more subways and tunnels are being constructed under complex geological conditions in coastal cities. Such structures are usually shallowly buried in soft ground. Their construction inevitably involves undercrossing a river, inducing ground movement, and leading to damage to nearby structures, which will be more serious in soft soil. Thus, exploring the influence of a river on tunnelling-induced deformation in costal soft soil is of great significance for controlling excessive settlement and protecting surrounding buildings.

Surface settlement induced by tunnelling has been extensively studied by various approaches. Empirical methods have been widely used. Peck (1969) proposed an empirical formula in the form of a Gaussian function. Other scholars modified the Peck formula by considering different influencing factors of surface settlement, e.g., soil type (O'Reilly and New, 1982), multiple tunnelling (Suwansawat and Einstein, 2007), and permeability of the soil (Tang et al., 2021). Due to a lack of field data, researchers usually rely on numerical modelling (Hajjar et al., 2015; Shahin et al., 2016; Goh et al., 2020) and physical modelling (Mair, 1996; Chapman et al., 2006, 2007; Divall, 2013) to study the movements caused by tunnelling.

✉ Xiao-wu TANG, tangxiaowu@zju.edu.cn
Jia-xin LIANG, https://orcid.org/0000-0001-6346-9883
Xiao-wu TANG, https://orcid.org/0000-0002-0916-8761

Received Dec. 30, 2021; Revision accepted Mar. 17, 2022; Crosschecked June 13, 2022

When constructed under a river, a tunnel will inevitably destroy the balance of the original groundwater seepage and stress fields. This causes difficulties with tunnel face stability (Höfle et al., 2008; Liu et al., 2018, 2021) and ground deformation (Cesano et al., 2000; Day, 2004; Huang and Zhang, 2004). Groundwater seepage causes excess pore water pressure to dissipate, which ultimately leads to soil consolidation and settlement in saturated soils of low permeability (Soga et al., 2017; Wan et al., 2019). Groundwater seepage is the main reason for excessive settlement (Yoo et al., 2012) and a sharp increase in surface settlement (Tang et al., 2017). The analysis of excess pore water pressure is useful for the control of ground deformation. It provides optimization advice for support pattens during the tunnelling process. For example, the support pressure should be set larger than the normal condition to maintain tunnel face stability (Liang et al., 2021), and more reinforcement should be applied before tunnel construction (Cattoni et al., 2016). A cofferdam is also considered as a way to reinforce the soil and reduce the deformation caused by construction (Ma, 2015; Xu and Liang, 2015).

Previous studies generally focused on the excess pore water pressure caused by excavation. Broere (2003) obtained the fluctuation characteristics of pore pressure during the tunnelling process. Wei et al. (2012) and Xu and Bezuijen (2018) proposed a pore water pressure distribution formula induced by tunnel excavation. The effect of soil and the tunnel construction method on pore water pressure was also studied. Zhou et al. (2018) and Li et al. (2019) established a 3D fluid-solid full coupling model to predict the pore water pressure around tunnels. However, many tunnels are constructed that cross a river in coastal cities. Construction across rivers will inevitably lead to groundwater seepage. The excess pore water pressure caused by groundwater seepage induced by a river has rarely been studied. Sahoo and Kumar (2019) considered the influence of groundwater seepage on support pressure using the finite element limit method. However, the deformation caused by groundwater seepage in the tunnelling process and the construction of a cofferdam has seldom been studied by both in-situ measurements and numerical analysis. It is of great significance to study the influence of different settlement and changes in excess pore water pressure within and outside a river area of influence and the impact of cofferdam construction and precipitation above the river on surface deformation.

In this study, the research region was divided into two parts, namely inside the river-affected area and outside the river-affected area, according to the monitoring data of the Zizhi Tunnel project. Different development laws of the surface settlement and its relationship with the vault settlement were analyzed and summarized. A numerical model was established by considering various reinforcements (e.g., a large-pipe shed and grouting pipes) to investigate the ground deformation in the whole excavation process. The distribution of the excess pore pressure both inside and outside the river-affected area, and the way it influences the surface settlement, were also analyzed using the numerical model. The effect of a cofferdam on the control of excessive settlement inside the river-affected area was studied.

2 Project overview

The Zizhi Tunnel is located in the western area of Hangzhou, China, and was divided into six sections during construction. The section selected for research was the first section, which is located near the north exit of the tunnel, surrounded by dense residential blocks and commercial buildings. The geological conditions of the research area, the design of the tunnel and cofferdam, and the measurement methods are introduced in this section.

2.1 Geological conditions

This study focused mainly on the west line of the twin tunnels. More information about the tunnel can be found in (Tang et al., 2021). Fig. 1 shows a typical longitudinal profile of the west line of the twin tunnels. The Yanshan River traverses above the tunnel. The tunnel excavation occurred mainly in a silty clay mixed gravel layer. Detailed geotechnical properties of each soil layer are listed in Table 1. The static water level is 0.6–3.5 m, with annual variation of 1–2 m.

2.2 Tunnel and cofferdam design

The tunnel was constructed using the cross diaphragm (CRD) method. During the excavation of the east and west lines, the face of the tunnel was divided into four parts (I, II, III, and IV), which were excavated

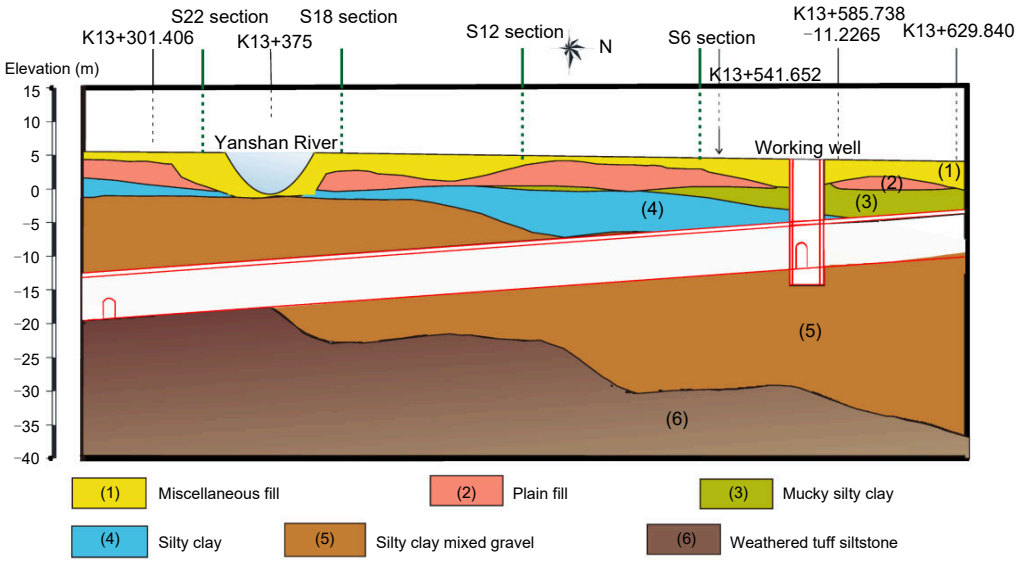

Fig. 1 Typical longitudinal profile (unit: m)

Table 1 Geotechnical properties of soil layers

Soil layer	γ (kN/m^3)	e	E_s (MPa)	υ	c (kPa)	φ (°)	k_v (cm/s)	k_h (cm/s)
(1)	17.5	0.783	2.6	0.33	0	10.0	4.0×10^{-3}	5×10^{-3}
(2)	18.4	0.875	3.5	0.35	10	12.0	6.5×10^{-4}	8×10^{-4}
(3)	17.6	1.245	2.5	0.45	11	9.5	4.0×10^{-7}	5×10^{-7}
(4)	19.4	0.721	6.0	0.41	35	16.0	2.0×10^{-7}	3×10^{-7}
(5)	19.8	0.601	10.0	0.38	45	17.0	6.0×10^{-6}	8×10^{-6}

γ: unit weight; e: void ratio; E_s: modulus of compressibility; υ: Poisson's ratio; c: cohesion; φ: internal friction angle; k_v: vertical permeability coefficient; k_h: horizontal permeability coefficient

in sequence (Fig. 2). After the excavation of each cross-section, except for the reinforcement around the tunnel, the vertical and transverse support structures of the central diaphragm were constructed to ensure the stability of each tunnel face. For the first 100 d of excavation, to ensure the stability of the stratum and reduce the mutual interference between the twin lines, a large distance between the west line and the east line was maintained. The west line was constructed ahead of the east line by 8–12 m. The four parts of the tunnel face of the east and west tunnels were kept at a certain distance: 10–12 m between parts I and II, 10–25 m between parts II and III, and 6–10 m between parts III and IV. The speed of the CRD method is 1 m/d. During the 100–120 d of tunnel excavation, the construction of the east and west line tunnels was adjusted to keep the excavation process consistent. After 120 d of excavation, the upper parts I and II of the east and west lines were excavated at the same pace, and the lower parts III and IV were excavated at the same pace. The interval between the upper and lower parts was 4–5 m, and the speed of construction was increased to 1.5 m/d.

A detailed description of the different support parameters can be found in Fig. 2 and Table 2. The advanced support included a large-pipe shed and grouting. The primary lining consists of shotcrete and steel arches. The secondary lining consists of reinforced concrete. Between the two linings is a waterproofing membrane. The large-pipe shed reinforcement is 9 m long with a diameter of 89 mm and a wall thickness of 6 mm, with a spacing of 30 cm. The small grouting pipes installed in the longitudinal direction are 4.5 m long with a spacing of 30 cm, while those along the cross-section direction are 3.5 m long with a spacing of 1 m. For the primary lining, the thickness is 30 cm, the type of the steel arch is I22a, and the compressive strength of the shotcrete is 25 MPa. For the secondary lining, the thickness is 60 cm and the compressive strength of the cast-in-place concrete is 35 MPa. Both the temporary middle wall and the invert consist of I18 steel beams.

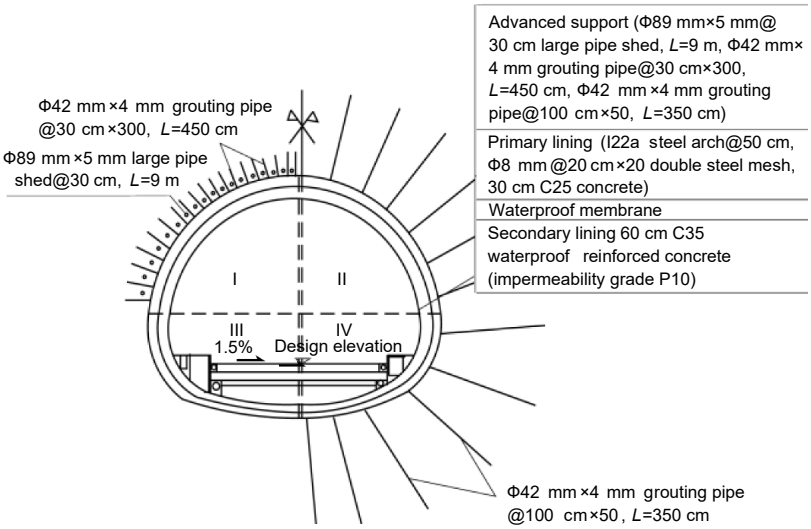

Fig. 2 Construction steps and support parameters of the CRD method (*L*: length)

Table 2 Summary of the support patterns

Item		Description
Advanced support	Large-pipe shed	Length: 9 m; thickness: 6 mm; Φ89 mm×5 mm@30 cm
	Grouting pipe (longitudinal direction)	Length: 4.5 m; Φ42 mm×4 mm@30 cm×300
	Grouting pipe (cross-section direction)	Length: 3.5 m; Φ42 mm×4 mm@100 cm×50
Primary lining	Steel arch	I22a@50 cm
	Steel mesh	Double layer; Φ8 mm@20 cm×20
	Concrete	Shotcrete: C25; thickness: 30 cm
Secondary lining	Concrete	Reinforced concrete: C35; thickness: 60 cm

The cross-section of the arrangement of the cofferdam and piles where the Zizhi Tunnel passes through the river is shown in Fig. 3. The width of the cross-river section of the tunnel is about 30 m. The constant water level of the river is 1.67 m. Before the tunnel crosses the river, clay cofferdams were constructed to block the water at a distance of 20 m from the upstream and downstream of the river, and diversion pipes were used to divert the river. During the construction of the cofferdam, two rows of high-pressure jet grouting piles with a diameter of 800 mm, and Larsen steel sheet piles, were constructed at a distance of 8 m from the upstream and downstream of the Zizhi Tunnel to block the water.

2.3 Measurement arrangement

Surface settlement and vault settlement were measured in the field using the DINI03 electronic level made by the Trimble Company, the USA. The measured data were automatically collected by the DINI03 electronic level device and could be transferred to a personal computer by using a USB flash disk. The data related to this study were selected and post-processed using Origin.

A total of 28 surface settlement monitoring sections within 300 m of the selected research area are shown in Fig. 4. For a better study of the influence of the river on the monitoring data, the research region was divided into two parts (Tang et al., 2021): inside the river-affected area (S16–S26) and outside the river-affected area (S1–S15 and S27–S28). The river-affected area was 45 m from the river center as the boundary, which is three times the width of the river (15 m). Outside that distance (45 m), the groundwater seepage effect caused by the river could be regarded as negligible. The vault settlement was measured correspondingly every 10–15 m to analyze the relationship of the vault settlement to the ground surface settlement.

3 Measured settlements

The surface settlements were measured during a period of about five months. The measured data

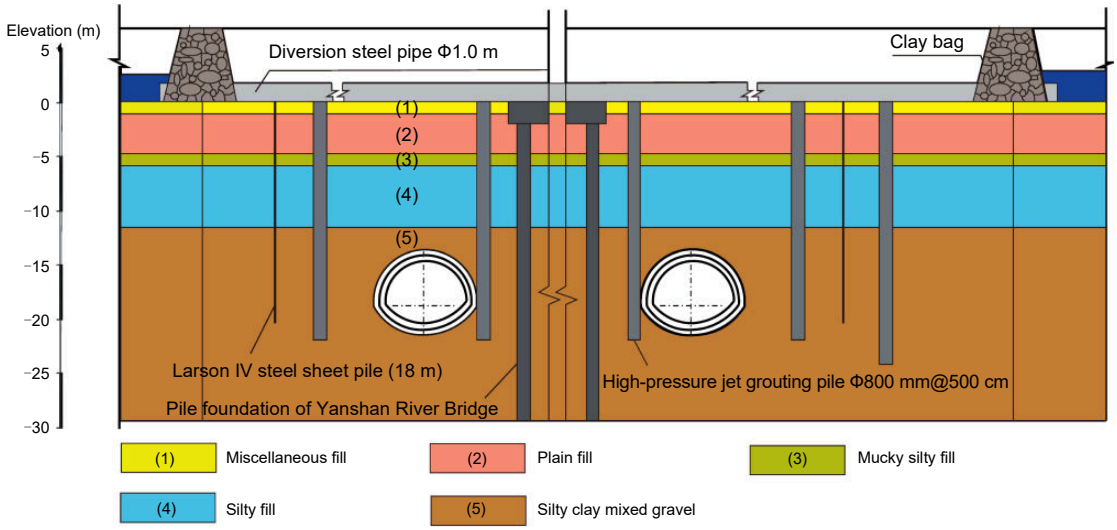

Fig. 3 Cross-section of the arrangement of the cofferdam and piles

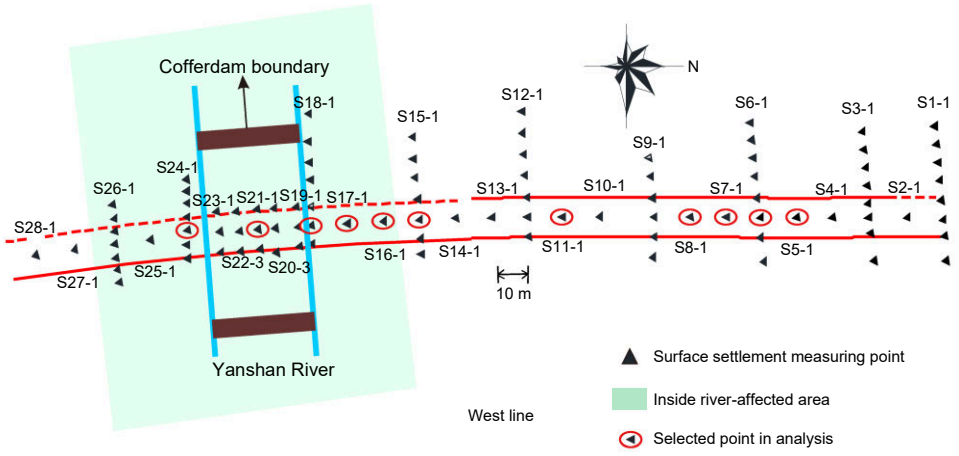

Fig. 4 Layout of monitoring points

represent only the settlements that developed after the installation of the settlement points. The surface and vault settlements of a single point are analyzed in this section.

3.1 Ground deformation of a single point in the center of the tunnel

Through the study of the development of surface settlement over time, we found that considering the relative position of the tunnel face and excavation face, the development of surface settlement could be divided into three stages: (1) the tunnel face is $1.0H_t$ away from the excavation face, where H_t is the tunnel height; (2) the tunnel face continues to move to the excavation face; (3) the tunnel face leaves the excavation surface and continues to move forward. The development of the surface settlement of the tunnel was affected by the river and the construction of the cofferdam, and showed different deformation laws within and outside the river-affected area.

Outside the river-affected area, taking a series of measurement points (S5-1, S6-6, S7-1, S8-1, S11-1) (Fig. 5), the development law of surface settlement over time could be analyzed. The trend of settlement development could be divided into three stages (taking S5-1 as an example): a slow growth stage before excavation, a rapid growth stage during excavation, and a gradual convergence stage after excavation. In the first stage, the increase of surface settlement was relatively slow due to the long distance between the tunnel face and the excavation surface. In the second

stage, the settlement grew faster (average 2 mm/d) due to the tunnel excavation. In the third stage, the surface settlement increased slowly until it converged, as the tunnel face became farther away from the excavation face.

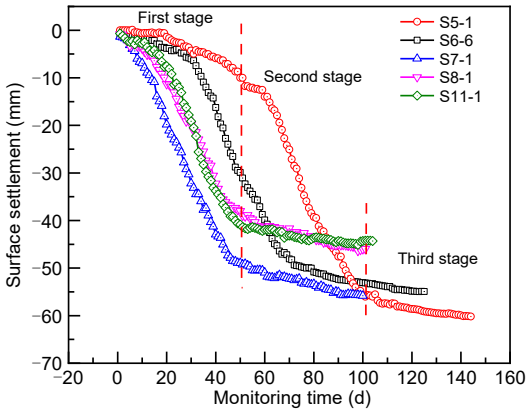

Fig. 5 Development of surface settlement outside the river-affected area

Within the river-affected area, measurement points S16-1, S17-1, S18-6, S21-5, and S24-5 were analyzed. From Fig. 6, taking S24-5 as an example, it can be seen that the surface settlement of the measuring points within or outside the river-affected area showed similar trends in the first and second stages, with a smaller increase of settlement in the second stage (1.5 mm/d). There was a difference in the third stage when the surface settlement had not completely converged after 90 d, but continued to increase. The rate of convergence was slower inside than that outside the river-affected area. The existence of the river and the groundwater drawdown during the construction of the

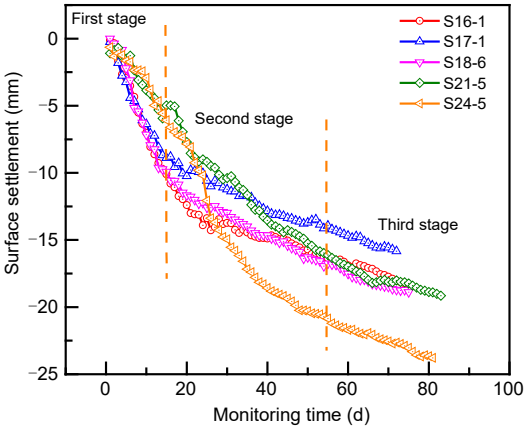

Fig. 6 Development of surface settlement inside the river-affected area

cofferdam had an impact on the development of the surface settlement, slowing the increase in settlement and extending the time taken to stabilize. This is because the existence of the river meant that surface settlement was affected not only by soil loss due to the stress release caused by tunnel excavation, but also by the deformation caused by groundwater seepage.

3.2 Comparison of ground surface settlement and vault settlement

Figs. 7a and 7b show the relationship between the surface settlement and vault settlement in two different kinds of monitoring sections: S6 and S7 outside the river-affected area, and S18 and S21 within the river-affected area. Two types of development laws on the surface settlement could be observed under the influence of the river. In the early stage, the rate of increase in the vault settlement was greater than that of

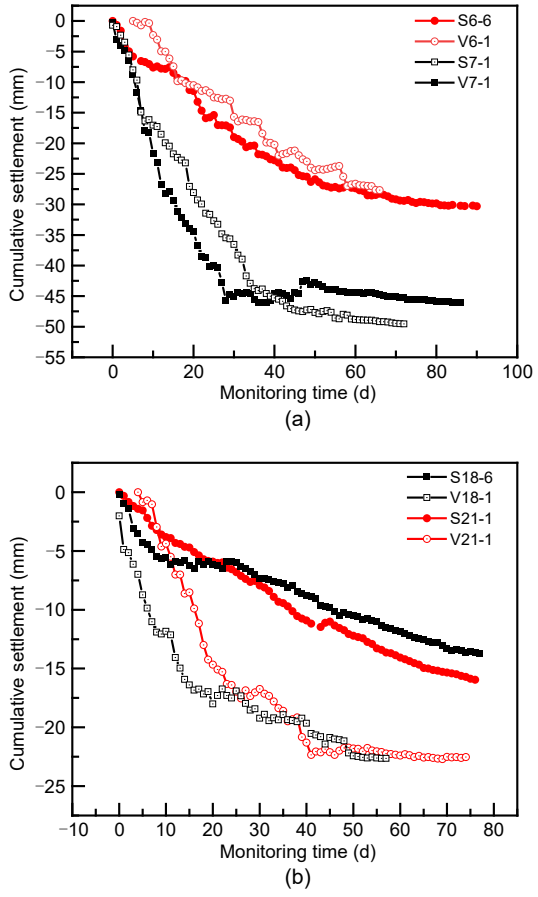

Fig. 7 Comparison of surface settlement and vault settlement development: (a) outside the river-affected area; (b) inside the river-affected area (V indicates the vault settlement measurement point)

the surface settlement. As the distance between the tunnel face and the monitoring section increased, the rate of increase in the vault settlement declined faster than that of the surface settlement. Fig. 7a shows that outside the river-affected area (S6 and S7), the vault and the surface settlement increased at a similar rate and tended to be stable at the same time. Fig. 7b shows that within the river-affected area (S18 and S21), after the vault settlement was stable, the surface settlement continued to increase. During construction, vault settlement was induced by the soil loss of from excavation. The asynchronization of the sinking rate and stability of the vault settlement and the surface settlement inside and outside the river-affected area indicated the influence of the river. The continuous growth of surface settlement was caused by the groundwater seepage induced by construction undercrossing the river.

From the above analysis, it can be seen that for a single point in the center of the tunnel, the development laws of the surface settlement inside and outside the river-affected area differed: the settlement increased more slowly in the second stage and continued to increase without convergence inside the river-affected area. The surface settlement in the river-affected area developed more slowly than the vault settlement, and continued to develop and differed greatly from the vault settlement. This may be due to the existence of the river. When construction undercrosses a river in soil with low permeability, groundwater seepage will cause pore pressure redistribution of the surrounding saturated silty clay mixed gravel layer, causing further consolidation and settlement (Yoo, 2016; Tang et al., 2017). The excess pore pressure caused by the construction of the tunnel and the cofferdam needs more time to dissipate. This is the main reason for the consolidation, and will be analyzed in Section 4.

4 Numerical modeling

The monitoring data showed the river had an impact on surface settlement, and there were different development laws for surface settlement within and outside the river-affected area. The mechanism of interaction between the tunnelling and the groundwater was explored using a numerical model related to the distribution and variation of excess pore water pressure. The excess pore water pressure is difficult to measure realistically, so numerical analysis was considered an effective way to reveal how the river and cofferdam influenced the surface settlement.

According to the engineering geology and construction conditions, a 3D numerical model of Zizhi Tunnel was constructed using Plaxis 3D to study the development law of surface settlement of twin tunnel construction. The following section describes the material properties, constitutive models, and construction method adopted in the finite element model.

4.1 Geometry of the model

The model has a length of 140 m, a width of 80 m, and a height of 60 m (Fig. 8). The distance between the central axis of the tunnel and the boundary of the model is $4.2H_t$, and the distance between the bottom of the tunnel and the bottom boundary of the model is $1.8H_t$. The grid is divided into mixed cells with 395728 elements and 533451 nodes.

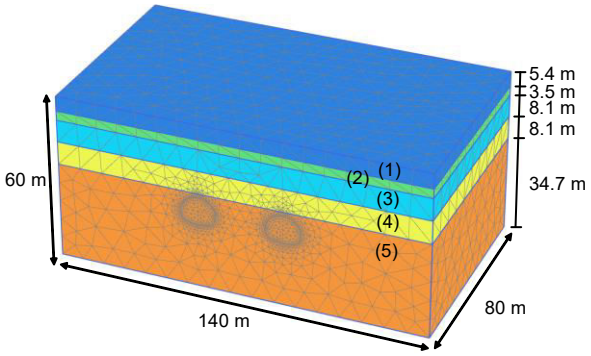

Fig. 8 Overview of the numerical model

4.2 Material properties and constitutive models

In actual construction, the stiffness of the soil decreases as the strain of the soil increases. The strength parameters of the soil used in the numerical simulation analysis were all from experimental results from tests under a large strain. Therefore, to obtain better simulation results, it was necessary to select reasonable constitutive models and model parameters for different soil layers. Based on the different soil layers of the tunnel construction, the Mohr-Coulomb (MC) model, the hardening soil (HS) model, and the hardening soil with small strain stiffness (HSS) model were selected for numerical simulation. The constitutive models and values of soil parameters are shown in Table 3.

Table 3 Geotechnical properties of soil layers in numerical analysis

Soil layer	Constitutive model	γ (kN/m^3)	E_s (MPa)	E_{50}^{ref} (MPa)	E_{oed}^{ref} (MPa)	E_{ur}^{ref} (MPa)	c' (kPa)	φ' (°)	G_0^{ref} (MPa)	K_0	m	$\gamma_{0.7}$
(1)	MC	17.5	2.6	–	–	–	0	10.0	–	–	–	–
(2)	MC	18.4	3.5	–	–	–	10	12.0	–	–	–	–
(3)	HSS	17.6	–	2.7	2.25	18	10	27	63	0.5	0.8	0.0001
(4)	HS	19.4	–	6.48	5.4	43.2	8	28	–	0.5	0.8	–
(5)	HS	19.8	–	10.8	9	72	10	23	–	0.5	0.8	–

E_{50}^{ref}: secant stiffness in standard drained triaxial test; E_{oed}^{ref}: tangent stiffness for primary oedometer loading; E_{ur}^{ref}: unloading/reloading stiffness from drained triaxial test; c': effective cohesion; φ': effective friction angle; G_0^{ref}: reference shear modulus at very small strains; K_0: coefficient of lateral earth pressure (initial stress state); m: power for stress-level dependency of stiffness; $\gamma_{0.7}$: threshold shear strain

4.3 Tunnel construction and the application of supporting system

The numerical model of the tunnel and the supporting system is shown in Fig. 9. The grouting reinforcement area formed by the tunnel advanced support included a large-pipe shed and grouting pipes. They were simulated by changing the geotechnical parameters of the corresponding soil and adding the corresponding structural elements. The reinforcement range of the grouting area was simulated by soil elements with modified geotechnical parameters (Table 4). A beam unit was used for simulation of the large-pipe shed. The detailed parameters of structural elements can be found in Table 5.

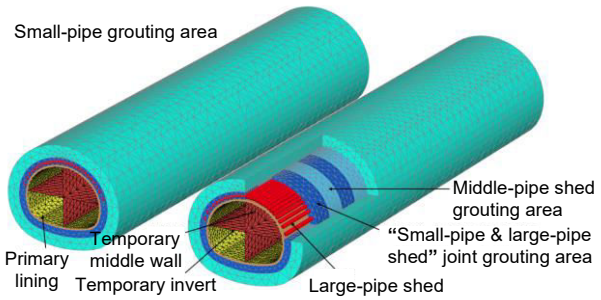

Fig. 9 Numerical model of the tunnel and the supporting system

The primary lining is composed mainly of shotcrete and steel arches. The steel arches were simulated by the equivalent method, and their elastic modulus was superimposed on the elastic modulus of concrete. The shotcrete was simulated by using plate and soil elements. First, the mechanical parameters of the plate element were set to calculate the force on the primary lining (Table 5). However, because the plate element is impermeable by default, a 30-cm thick soil element was set outside the plate element. The influence of the primary lining on seepage was simulated by inputting the permeability coefficient of the 30-cm thick soil element consistent with the original soil. The secondary lining included the temporary middle wall and the temporary invert. They were all simulated by plate elements. The detailed information can be found in Table 5.

The construction of the cofferdam was realized by drawdown of the water level of the river. The high-pressure jet grouting piles in Fig. 10 were simulated by pile elements with embedded beams. The mechanical parameters of high-pressure jet grouting piles are shown in Table 6, and the construction model is shown in Fig. 10.

5 Numerical analysis inside and outside the river-affected area

After the soil around the shield tunnel is disturbed by the shield construction, an excess pore water pressure zone is formed around the shield tunnel, which influences the stability of the tunnel face. After construction, the pore water pressure around the tunnel drops. When the excess pore water pressure gradually dissipates, the pore water is gradually discharged, causing ground settlement, which is known as consolidation settlement. It can be seen that the key to the analysis of long-term consolidation settlement lies in the study of the pore water pressure around the tunnel. Based on the numerical analysis, we analyzed the distribution of the excess pore water pressure and its influence on the settlement of the soil around the tunnel, and compared the results with the monitoring data to verify their reliability.

5.1 Outside the river-affected area

The cross-section at y=40 m was selected to study the development law of surface settlement. Fig. 11

Table 4 Geotechnical properties of soil elements in numerical analysis

Grouting type	γ (kN/m^3)	e	E_s (MPa)	υ	c (kPa)	φ (°)	k_v (cm/s)	k_h (cm/s)
Longitudinal grouting pipe & large-pipe shed	25	0.15	50	0.33	135.0	21	1.0×10^{-7}	1.5×10^{-7}
Large-pipe shed	24	0.25	35	0.35	90.0	20	1.5×10^{-7}	2.3×10^{-7}
Cross-section grouting pipe	23	0.30	25	0.38	67.5	19	2.0×10^{-7}	3.0×10^{-7}

Table 5 Geotechnical properties of structure elements used in numerical analysis

Structure type	γ (kN/m^3)	E (MPa)	υ	t (cm)	A (cm^2)	I_p (cm^4)
Large-pipe shed	48	93	0.25	–	13.195	233.579
Primary lining	25	28	0.20	30	–	–
Temporary middle wall & temporary invert	25	40	0.20	25	–	–

E: elastic modulus; t: thickness; A: cross-sectional area; I_p: polar moment of inertia

Table 6 Geotechnical properties of high-pressure jet grouting piles

Parameter	Value
γ (kN/m^3)	20
E (MPa)	200
υ	0.25
Diameter of the pile, d (mm)	800
Spacing, L_s (mm)	500
Side friction, f_r (kN/m)	1200

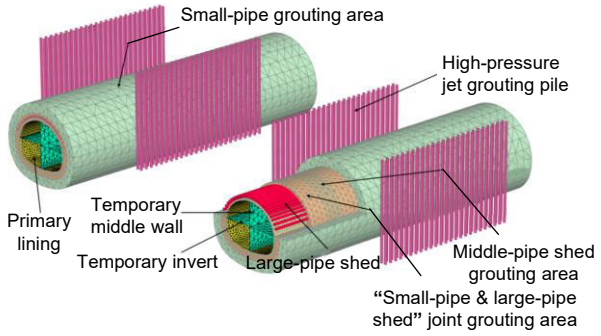

Fig. 10 Reinforcement of cofferdam

shows a comparison between the simulation results at the corresponding position of S6-6 and the monitoring data. It can be seen that the numerical model could simulate the three stages of the development law of surface settlement outside the river-affected area. The credibility of the model was verified. The simulated settlement was larger than that of the monitoring data, especially in the third stage. This was because the secondary lining after the tunnel excavation was not simulated in the numerical model, which led to a larger settlement increasing with time.

Fig. 12 shows that the excess pore pressure P_{excess} generated during the CRD excavation process of the

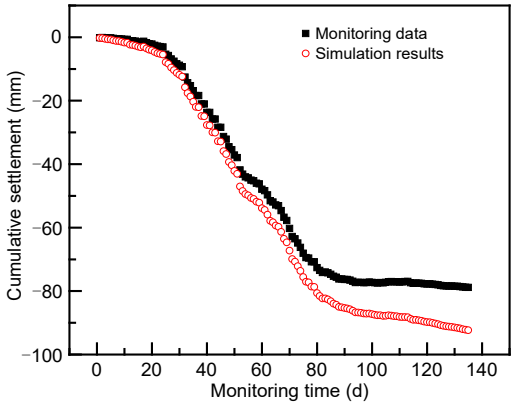

Fig. 11 Comparison of monitoring data and simulation results for settlement of S6-6

tunnel was distributed in a large range before and after the tunnel excavation face. The largest negative excess pore pressure $P_{negative}$ (about 18 kPa) was distributed in the range of $1.0H_t$–$3.0H_t$ behind tunnel faces III and IV, and in the range of $1.0H_t$–$2.0H_t$ in front of tunnel faces I and II. The positive excess pore pressure $P_{positive}$ was distributed in the interval during which the upper face of the tunnel had been excavated, but the lower face had not. The maximum $P_{positive}$ was distributed at the bottom of the tunnel, between the upper and lower faces.

Fig. 12 shows that when the tunnel was excavated outside the river-affected area, apart from the excess pore pressure of the surrounding soil caused by excavation at the tunnel face, excess pore pressure was also present in a certain range behind the excavation face. Therefore, after the excavation of the tunnel face is completed, corresponding support measurements must be constructed in time to control the excessive deformation of the surrounding soil.

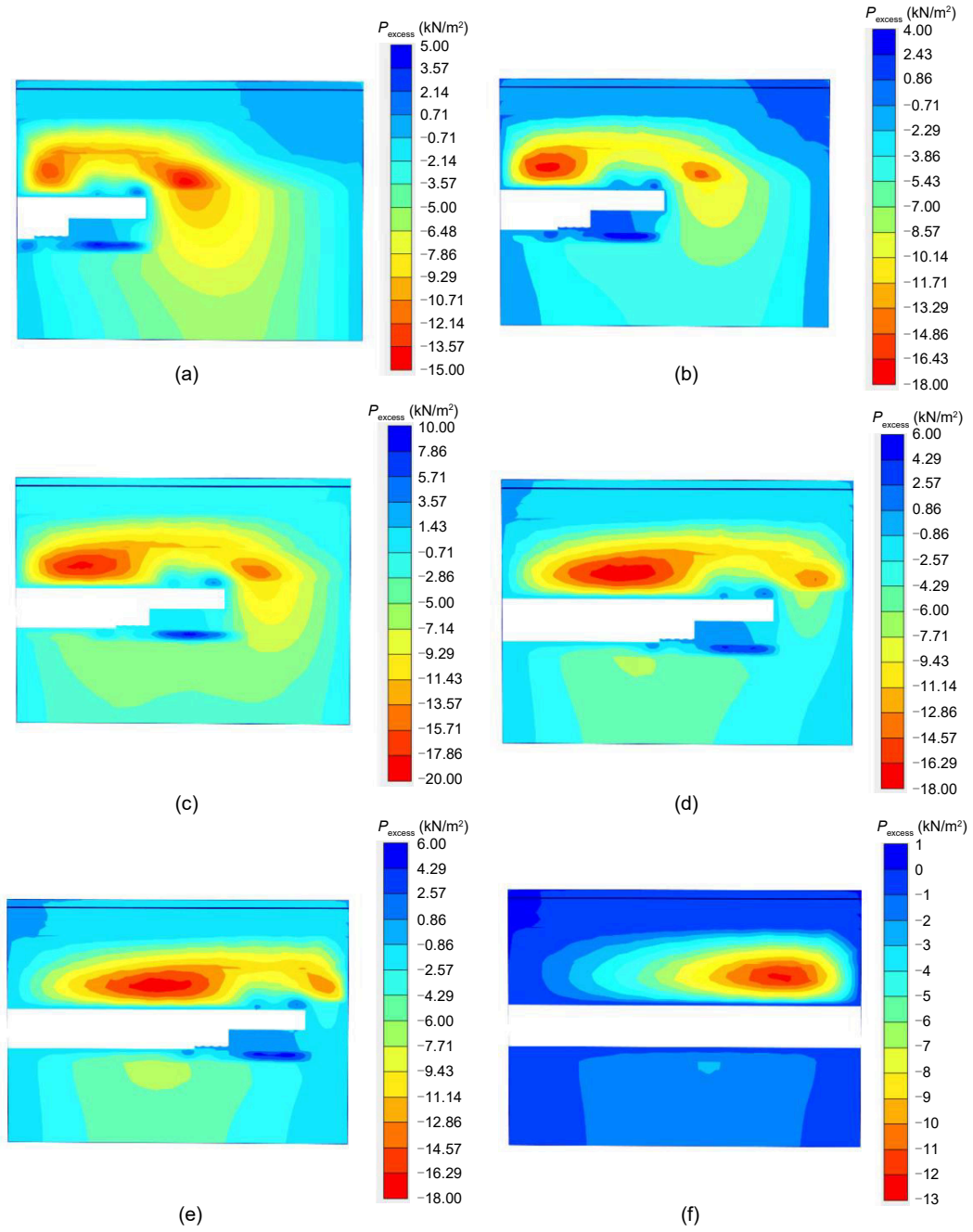

Fig. 12 Excess pore pressure and distribution cloud map outside the river-affected area: (a) the 15th excavation step; (b) the 20th excavation step; (c) the 25th excavation step; (d) the 31st excavation step; (e) the 35th excavation step; (f) the 55th excavation step

5.2 Inside the river-affected area

5.2.1 Numerical analysis of twin tunnels without groundwater drawdown during construction of the cofferdam

To explore the influence of groundwater drawdown during the construction of the cofferdam on the surface settlement, the water level above the river was restored to the normal level of 1.67 m. The new numerical model is shown in Fig. 13.

The cross-section at y=32 m was selected to study the development law of surface settlement. Fig. 14 shows a comparison between the simulation results at the corresponding positions of S18-6 and the monitoring

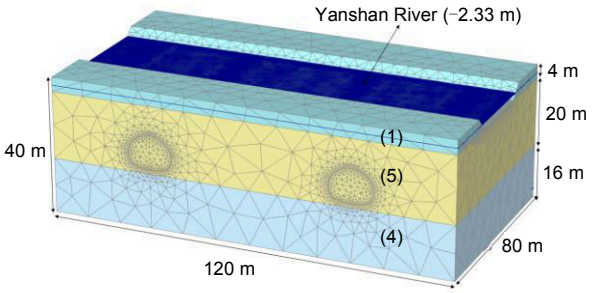

Fig. 13 Numerical model without cofferdam

data. The numerical result of the original water level was larger than that of the monitoring data. The maximum settlement was 40 mm, which is 25 mm larger than the actual settlement—an increase of 167%.

The variation in the P_{excess} with the tunnel excavation under the original water level of the river is shown in Fig. 15. The distribution range of the P_{excess} generated by excavation of the tunnel in the cross-river section decreased. The $P_{negative}$ was concentrated in the $1.0H_t$–$1.5H_t$ square area in front of the tunnel face, and within $1.0H_t$ behind the tunnel excavation face. The maximum $P_{negative}$ (about 12 kPa) was in the front section of the tunnel face. The $P_{positive}$ distributed

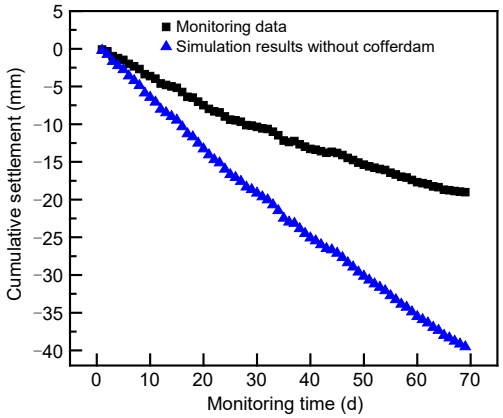

Fig. 14 Comparison of settlement of S18-6 without the cofferdam

mainly in front of tunnel faces III, IV, and the bottom of the tunnel.

5.2.2 Numerical analysis of twin tunnels with groundwater drawdown during construction of the cofferdam

As for the model without cofferdam construction, the cross-section at y=32 m of the model was selected to be compared and analyzed. Fig. 16 shows

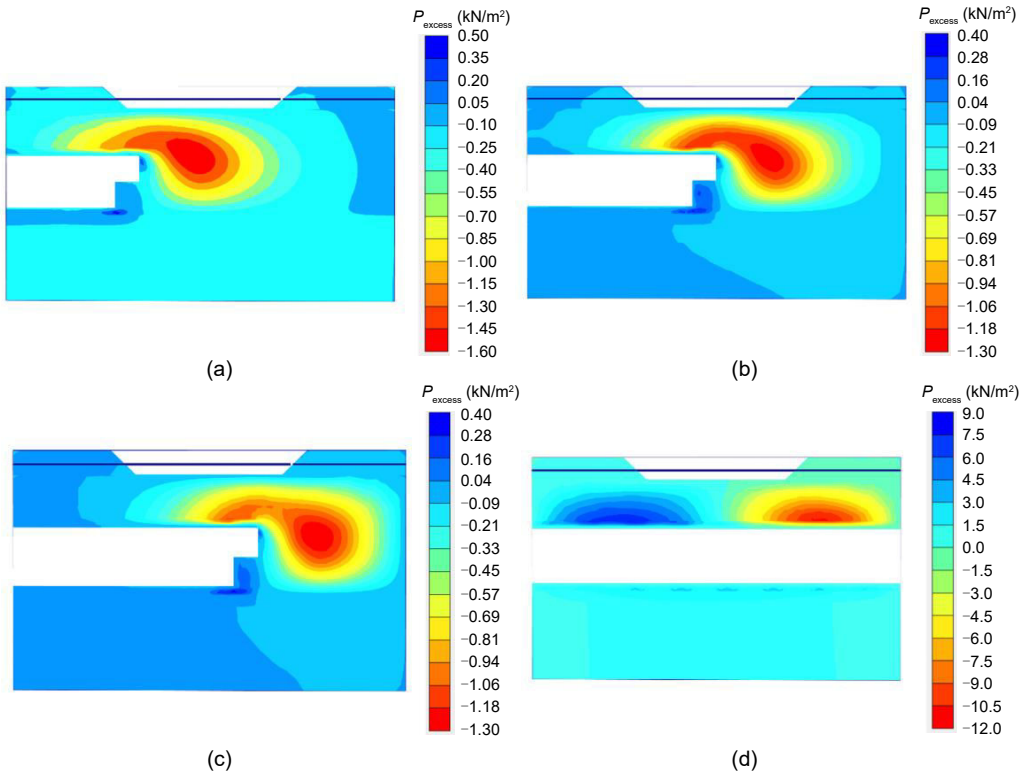

Fig. 15 Excess pore pressure and distribution cloud map without the cofferdam: (a) the 11th excavation step; (b) the 16th excavation step; (c) the 20th excavation step; (d) the 36th excavation step

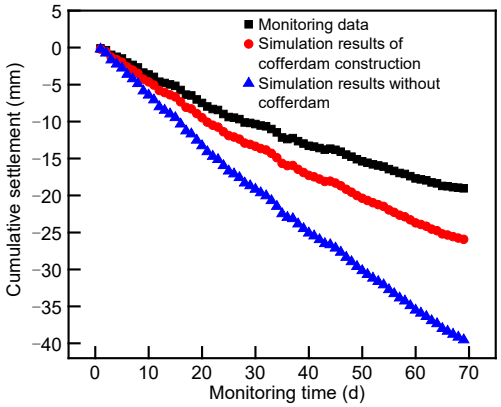

Fig. 16 Comparison of settlement of S18-6 with the cofferdam

the comparison between the simulation results at the corresponding positions of S18-6 and the monitoring data. The numerical model gave a better representation of the development law of surface settlement. Both the numerical simulation and the monitoring data maintained continuous growth of settlement without convergence after 70 d. The numerical results showed that the settlement induced by consolidation increased with time, which was consistent with the monitoring data. However, the settlement of the numerical simulation with the cofferdam was always larger than that of the monitoring data. This may be due to the addition of sealing measures applied to the tunnel lining during the actual construction to prevent groundwater leakage, which were not simulated in the numerical model. The increase in error between the simulation and measurement with the service time may have been induced by two factors: the survival time of S18-6 being no longer enough to make the surface settlement stabilize, or the degradation of the shear modulus of soil with the HSS model.

As for the comparison between simulation results with and without the cofferdam, the maximum numerical simulated settlement with the cofferdam (25 mm) was much smaller than that without the cofferdam (40 mm). The construction of the cofferdam could effectively reduce the excessive ground settlement by about 60%.

The variation of the P_{excess} within the river-affected area with the cofferdam is shown in Fig. 17. The P_{excess}

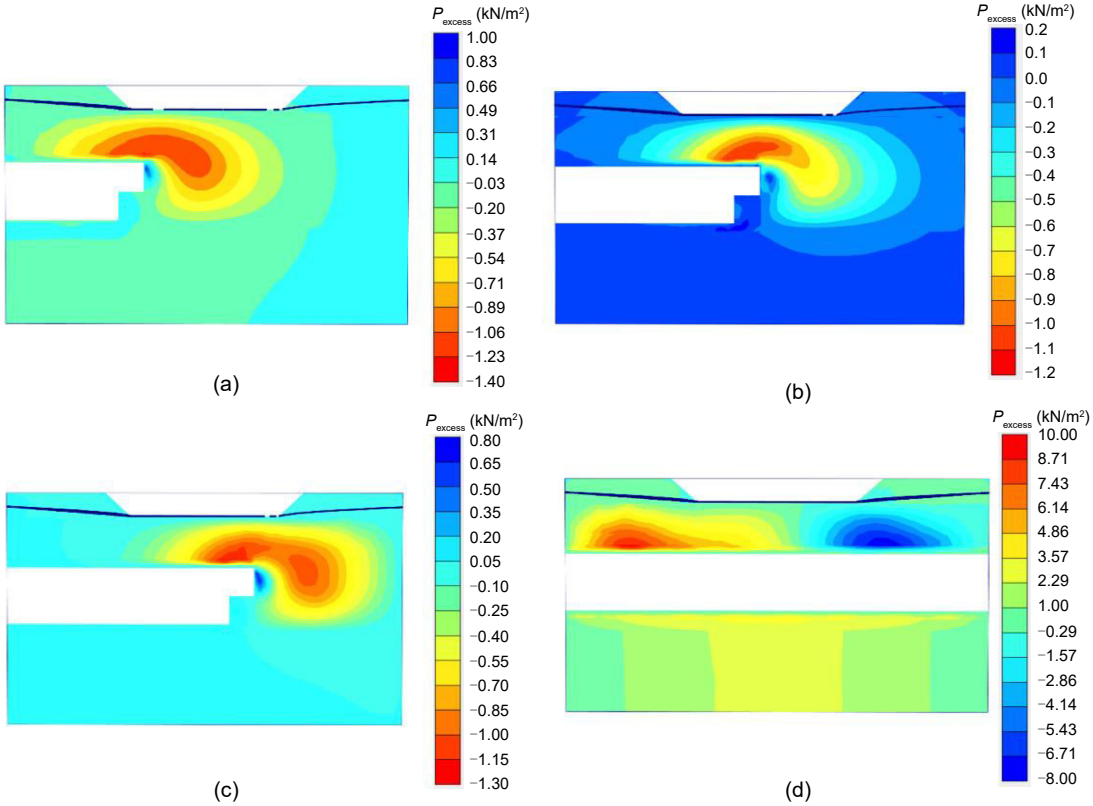

Fig. 17 Excess pore pressure and distribution cloud map with the cofferdam: (a) the 11th excavation step; (b) the 16th excavation step; (c) the 20th excavation step; (d) the 36th excavation step

was concentrated mainly in a certain range before and behind the excavation face. The $P_{negative}$ was concentrated at $1.0H_t$ to $2.0H_t$ before and behind the tunnel face. When crossing the river, the $P_{negative}$ reached its maximum of about 8 kPa. The $P_{positive}$ was distributed mainly at $0.5H_t$ before the upper tunnel face parts I and II, and then at $0.5H_t$ before the lower tunnel face parts III and IV. The excess pore pressure in the river-affected area was still present after the tunnel excavation was completed (Fig. 17d). The excess pore pressure dissipated slowly, delaying consolidation of the soil, leading to non-convergence in the later part of development of the settlement.

The excess pore water pressure caused by the excavation was more concentrated within the river-affected area than outside the river-affected area, and concentrated mainly before the excavation face. This would result in problems with tunnel face stability. Therefore, certain support measures, such as higher support face pressure and slower excavation speed, should be applied before the tunnel face when a tunnel is excavated in an area where the seepage field changes.

Cofferdam construction measures of lowering the water level can reduce the surface settlement by 39%. The construction of the cofferdam over the river can also reduce the consolidation settlement caused by excess pore water pressure and accelerate the time of consolidation. Therefore, when there is a river above a tunnel, if the corresponding measures of lowering the water level of the river are not taken, the soil around the excavation face should be pre-grouted and reinforced to reduce soil deformation around the tunnel face.

6 Conclusions

Based on the Zizhi Tunnel project, in this paper we presented a case study of the development law of the surface settlement, as well as its relationship with vault settlement during the construction of shallow-buried twin tunnels undercrossing a river in soft soil, which has different effects on the settlement inside and outside the river-affected area. A numerical model was established to explore the way that the river influences the surface settlement. The impact of the distribution of excess pore water pressure during the excavation and construction of the cofferdam was studied. The main findings can be summarized as follows:

1. The development laws of the surface settlement were different inside and outside the river-affected area. For a single point on the center line, the law of surface settlement over time could be divided into three stages, both inside and outside the river-affected area. There was a difference in the third stage in which the surface settlement had not completely converged after 90 d, but continued to increase within the river-affected area. Within the river-affected area, there was an asynchronization of the sinking rate and stability of vault settlements and surface settlements.

2. A numerical model was established to explore the causes of the different development laws of the surface settlement inside and outside the river-affected area. The numerical results showed good agreement with the monitoring data, which proves the rationality of the numerical model. Based on the numerical model, the excess pore water pressure was analyzed, including its distribution and value. Outside the river-affected area, the main factor that influenced the stability of the tunnel face and the development of surface settlement was the excavation of the upper face of the tunnel. Inside the river-affected area, apart from the settlement caused by excavation, the consolidation settlement resulting from the dissipation of excess pore water pressure caused by cofferdam construction above the river was also important, extending the time needed for settlement to converge.

3. Outside the river-affected area, the negative excess pore water pressure was distributed mainly in the range of $1.0H_t$–$3.0H_t$ behind the tunnel face, and $1.0H_t$–$2.0H_t$ in front of the tunnel face. Inside the river-affected area, the negative excess pore pressure was distributed in the range of $1.0H_t$–$2.0H_t$ before and behind the tunnel face, which is more concentrated. The area that had the greatest impact on the stability of the tunnel face was distributed $1.0H_t$–$3.0H_t$ before the tunnel face. The construction of the tunnel cofferdam reduced the surface settlement by 39%, and the excess pore water pressure distribution generated by the construction of the cofferdam was more dispersed, which could reduce the tunnel construction risk. To better control the settlement caused by a tunnel undercrossing a river, reinforcements such as a cofferdam and pre-grouting support could be applied.

Acknowledgments

This work is supported by the Key Water Science and Technology Project of Zhejiang Province (No. RB2027) and

the Zhejiang Province Public Welfare Technology Application Research Project (No. LGG22E080002), China.

Author contributions

Xiao-wu TANG designed the research. Jia-xin LIANG and Yu-hang YE processed the corresponding data. Jia-xin LIANG wrote the first draft of the manuscript. Tian-qi WANG and Ying-jing LIU helped to organize the manuscript. Jia-xin LIANG and Tian-qi WANG revised and edited the final version.

Conflict of interest

Jia-xin LIANG, Xiao-wu TANG, Tian-qi WANG, Yu-hang YE, and Ying-jing LIU declare that they have no conflict of interest.

References

Broere W, 2003. Influence of excess pore pressures on the stability of the tunnel face. *In*: Saveur J (Ed.), (Re) Claiming the Underground Space. A.A. Balkema, Lisse, the Netherlands, p.759-765.

Cattoni E, Miriano C, Boco L, et al., 2016. Time-dependent ground movements induced by shield tunneling in soft clay: a parametric study. *Acta Geotechnica*, 11(6):1385-1399. https://doi.org/10.1007/s11440-016-0452-x

Cesano D, Olofsson B, Bagtzoglou AC, 2000. Parameters regulating groundwater inflows into hard rock tunnels—a statistical study of the Bolmen tunnel in Southern Sweden. *Tunnelling and Underground Space Technology*, 15(2):153-165. https://doi.org/10.1016/S0886-7798(00)00043-2

Chapman DN, Rogers C, Hunt L, 2006. Predicting the settlements above closely spaced triple tunnels constructions in soft ground. Geotechnical Aspects of Underground Construction in Soft Ground. Proceedings of the 5th International Conference of TC 28 of the ISSMGE, p.219-224. https://doi.org/10.1201/NOE0415391245.CH26

Chapman DN, Ahn SK, Hunt DVL, 2007. Investigating ground movements caused by the construction of multiple tunnels in soft ground using laboratory model tests. *Canadian Geotechnical Journal*, 44(6):631-643. https://doi.org/10.1139/t07-018

Day MJ, 2004. Karstic problems in the construction of Milwaukee's deep tunnels. *Environmental Geology*, 45(6):859-863. https://doi.org/10.1007/s00254-003-0945-4

Divall S, 2013. Ground Movements Associated with Twin-Tunnel Construction in Clay. PhD Thesis, City University London, London, UK.

Goh ATC, Zhang RH, Wang W, et al., 2020. Numerical study of the effects of groundwater drawdown on ground settlement for excavation in residual soils. *Acta Geotechnica*, 15(5):1259-1272. https://doi.org/10.1007/s11440-019-00843-5

Hajjar M, Hayati AN, Ahmadi MM, et al., 2015. Longitudinal settlement profile in shallow tunnels in drained conditions. *International Journal of Geomechanics*, 15(6):1-12. https://doi.org/10.1061/(ASCE)GM.1943-5622.0000447

Höfle R, Fillibeck J, Vogt N, 2008. Time dependent deformations during tunnelling and stability of tunnel faces in fine-grained soils under groundwater. *Acta Geotechnica*, 3(4):309-316. https://doi.org/10.1007/s11440-008-0075-y

Huang J, Zhang DL, 2004. Analysis of large deformation regularity in stratum above metro tunnel. *Rock and Soil Mechanics*, 25(8):1288-1292 (in Chinese). https://doi.org/10.3969/j.issn.1000-7598.2004.08.024

Li Z, Luo ZJ, Xu CH, et al., 2019. 3D fluid-solid full coupling numerical simulation of soil deformation induced by shield tunnelling. *Tunnelling and Underground Space Technology*, 90:174-182. https://doi.org/10.1016/j.tust.2019.03.020

Liang Y, Zhang J, Chen XY, 2021. The impact of excess pore pressure on the support stability of a shield when tunnelling in sand stratum. *KSCE Journal of Civil Engineering*, 25(8):3136-3145. https://doi.org/10.1007/s12205-021-0686-5

Liu W, Zhao Y, Shi PX, et al., 2018. Face stability analysis of shield-driven tunnels shallowly buried in dry sand using 1-*g* large-scale model tests. *Acta Geotechnica*, 13(1):1-13. https://doi.org/10.1007/s11440-017-0607-4

Liu W, Wu B, Shi PX, et al., 2021. Analysis on face stability of rectangular cross-sectional shield tunneling based on an improved two-dimensional rotational mechanism. *Acta Geotechnica*, 16(11):3725-3738. https://doi.org/10.1007/s11440-021-01219-4

Ma L, 2015. Application research of steel sheet pile cofferdam in water-pier reinforcement engineering. *Transportation Science & Technology*, (3):31-34 (in Chinese). https://doi.org/10.3963/j.issn.1671-7570.2015.03.011

Mair RJ, 1996. Settlement effects of bored tunnels. International Conference of Geotechnical Aspects on Underground Construction in Soft Ground, p.43-53.

O'Reilly MP, New BM, 1982. Settlements above tunnels in the United Kingdom–their magnitude and prediction. Proceedings of Tunnelling'82 Symposium, p.173-181.

Peck BR, 1969. Deep excavations and tunneling in soft ground. Proceedings of the 7th International Conference on Soil Mechanics and Foundations Engineering, p.225-290.

Sahoo JP, Kumar B, 2019. Support pressure for stability of circular tunnels driven in granular soil under water table. *Computers and Geotechnics*, 109:58-68. https://doi.org/j.compgeo.2019.01.005

Shahin HM, Nakai T, Ishii K, et al., 2016. Investigation of influence of tunneling on existing building and tunnel: model tests and numerical simulations. *Acta Geotechnica*, 11(3):679-692. https://doi.org/10.1007/s11440-015-0428-2

Soga K, Laver RG, Li ZL, 2017. Long-term tunnel behaviour and ground movements after tunnelling in clayey soils. *Underground Space*, 2(3):149-167. https://doi.org/10.1016/j.undsp.2017.08.001

Suwansawat S, Einstein HH, 2007. Describing settlement troughs over twin tunnels using a superposition technique.

Journal of Geotechnical and Geoenvironmental Engineering, 133(4):445-468.
https://doi.org/10.1061/(ASCE)1090-0241(2007)133:4(445)

Tang XW, Gan PL, Liu W, et al., 2017. Surface settlements induced by tunneling in permeable strata: a case history of Shenzhen Metro. *Journal of Zhejiang University-SCIENCE A (Applied Physics & Engineering)*, 18(10):757-775.
https://doi.org/10.1631/jzus.A1600522

Tang XW, Liang JX, Liu W, et al., 2021. Modification of peck formula to predict ground surface settlement of twin tunnels in low permeability soil. *Advances in Civil Engineering*, 2021:6698673.
https://doi.org/10.1155/2021/6698673

Wan MSP, Standing JR, Potts DM, et al., 2019. Pore water pressure and total horizontal stress response to EPBM tunnelling in London Clay. *Géotechnique*, 69(5):434-457.
https://doi.org/10.1680/jgeot.17.p.309

Wei XJ, Chen WJ, Wei G, et al., 2012. Research on distribution of initial excess pore water pressure due to shield tunnelling. *Rock and Soil Mechanics*, 33(7):2103-2109 (in Chinese).
https://doi.org/10.3969/j.issn.1000-7598.2012.07.028

Xu H, Liang ZG, 2015. Reinforcement technology of large-scale steel sheet pile cofferdam in soft foundation on the sea. *Construction Technology*, 44(17):120-123 (in Chinese).
https://doi.org/10.7672/sgjs2015170120

Xu T, Bezuijen A, 2018. Analytical methods in predicting excess pore water pressure in front of slurry shield in saturated sandy ground. *Tunnelling and Underground Space Technology*, 73:203-211.
https://doi.org/10.1016/j.tust.2017.12.011

Yoo C, 2016. Ground settlement during tunneling in groundwater drawdown environment–influencing factors. *Underground Space*, 1(1):20-29.
https://doi.org/10.1016/j.undsp.2016.07.002

Yoo C, Lee YJ, Kim SH, et al., 2012. Tunnelling-induced ground settlements in a groundwater drawdown environment–a case history. *Tunnelling and Underground Space Technology*, 29:69-77.
https://doi.org/10.1016/j.tust.2012.01.002

Zhou H, Gao Y, Zhang CQ, et al., 2018. A 3D model of coupled hydro-mechanical simulation of double shield TBM excavation. *Tunnelling and Underground Space Technology*, 71:1-14.
https://doi.org/10.1016/j.tust.2017.07.012